



Assessing the impacts of Amphan cyclone over West Bengal, India: a multi-sensor approach

Rajesh Kumar · Seema Rani ·
Pyarimohan Maharana

Received: 17 July 2020 / Accepted: 11 April 2021 / Published online: 19 April 2021
© The Author(s), under exclusive licence to Springer Nature Switzerland AG 2021

Abstract Landfall of the Amphan (very severe cyclonic storm) occurred at 1730 hrs Indian Standard Time (IST) on May 20, 2020, near the West Bengal (W.B.) coast of India. High wind speed, storm surge, and torrential rainfall-induced flooding caused devastation in W.B. The present study aims to analyse the impacts of Amphan cyclone on land use/land cover (LULC) such as built-up area, cropland, brick-kiln industries and vegetation cover of nine districts of W.B. namely, Bardhaman, Nadia, North 24 Parganas, South 24 Parganas, Purba Medinipur, Paschim Medinipur, Haora, and Kolkata. Flood extent has been mapped using Sentinel-1A and B interferometric

wide swath (IW) ground range detected (GRD) VV polarisation images dated May 22, 2020. The total actual flooded area covers 488 km² of the study area. For the pre-cyclone period, LULC classification and normalised difference vegetation index (NDVI) have been done using Sentinel-2B multispectral instrument (MSI) images dated May 14, 2020. Post-cyclone NDVI has been computed using Sentinel-2B MSI images dated June 3, 2020. Flood-affected cropland covers a large chunk (88.2%) of the total actual flooded area. Mean NDVI values of non-flooded and flooded cropland and vegetation cover have been reduced between May 14, 2020, and June 3, 2020. District, block and pixel-wise changes in pre- and post-cyclone NDVI values have also been analysed. This study helps planners and policy makers to understand the district-wise flooding behavior, severity of damage to cropland and vegetation cover and to plan restriction on high-value land use in flooded low-lying areas.

Keywords Amphan cyclone · SAR · LULC · NDVI · Sentinel-1

R. Kumar (✉)
Centre for the Study of Regional Development, Jawaharlal
Nehru University, New Delhi, India
e-mail: rajeshcsrd@gmail.com

R. Kumar
Department of Geography, Sikkim University, Gangtok,
Sikkim, India

S. Rani
Department of Geography, Institute of Science, Banaras
Hindu University, Varanasi, Uttar Pradesh, India

P. Maharana
School of Environmental Sciences, Jawaharlal Nehru
University, New Delhi, India

P. Maharana
Faculty of Science, Sri Sri University, Cuttack, Odisha,
India

Introduction

Tropical cyclones are one of the devastating natural disasters because they cause damage to vegetation, wild and human lives, public and private properties of the coastal and inland areas during landfall.

The tropical cyclones are termed by different names like hurricanes in the north-eastern Pacific and the Atlantic Ocean, typhoons in the west Pacific Ocean and tropical cyclones in the Indian and South Pacific Ocean (WHO, 2020). Tropical cyclones cause damage to landscape and lives due to severe winds, tornadoes, lightning, torrential downpour, storm surges and floods. In the last 50 years, 1,942 disasters are induced by tropical cyclones, killing 779,324 persons and causing USD 1,407.6 billion economic losses across the world (WMO, 2020) indicating its impact on the global as well as the regional economy. India is frequently affected by natural hazards such as floods, earthquakes, droughts, landslides and tropical cyclones. In the last few decades, rise in cyclonic activities over the Indian Ocean is attributed to climate change (Mishra, 2014; Sebastian & Behera, 2015). A sum of 103 severe cyclones has occurred on the east coast of India while only 24 cyclones on the west coast of India during 1891–2000 (NCRMP, 2020). About 5% of the total number of tropical cyclones of the world are originated from the Bay of Bengal (Alam & Dominey-Howes, 2015). Frequent tropical cyclones occur over the Bay of Bengal during November–May months (Singh et al., 2000). Twenty-four Paragana (North and South) and Medinipur (Purba and Paschim) coastal districts of West Bengal (W.B.) witnessed 35 and 34 cyclones during 1891–2002, respectively (NCRMP, 2020). The increasing frequency of cyclonic activities in India is a major issue for the disaster management and policy makers.

Natural disaster causes a loss of 2% of total India's gross domestic product (GDP) (World Bank, 2003). Besides financial loss, human lives are severely affected by such natural disasters. On an average, annually 370 million persons from coastal regions of India are vulnerable to tropical cyclones (NCRMP, 2020). More vulnerable cyclones occur in four Indian states such as Tamil Nadu, Andhra Pradesh, Odisha and W.B. and Puducherry Union Territory (UT) on the east coast and in Gujarat state on the west coast (Mohapatra et al., 2012). The northern part of the Indian Ocean namely, the Bay of Bengal and the Arabian Sea creates only 7% of the total number of cyclones of the world (Neumann, 1993) which cause devastation in coastal regions of India (Mohapatra et al., 2012).

This is important to assess the impact of the extremely severe cyclonic storm for the post-cyclone

management strategies. Tropical cyclones often cause severe damage to communication and transport systems due to severe winds and torrential rainfall leading to restricted traveling (Hoque et al., 2016). Therefore, the assessment of cyclonic storm-induced damage to vegetation, buildings and cropland is not feasible and quick by adopting the traditional field survey methods (Zhang et al., 2013). In the situation of disrupted communication and transport systems, remote sensing images from active and passive sensors are cost-effective and provide immense opportunity for assessing the impacts of cyclonic storms at varying spatial scales within a short period (Bhowmik & Cabral, 2013). The cyclones-induced damage to cropland, built-up areas, forest and its canopy along with flooded areas has been analysed using passive remote sensing images from the National Oceanic and Atmospheric Administration (NOAA) Advanced Very High Resolution Radiometer (AVHRR), Landsat Thematic Mapper (TM), Moderate Resolution Imaging Spectroradiometer (MODIS), QuickBird, Satellite Pours' Observation de la Terre (SPOT)-5, Landsat 8 and Sentinel-2 sensor (Ramsey et al., 2001; Staben & Evans, 2008; Negrón-Juárez et al., 2014; Hoque et al., 2016; Hu & Smith, 2018). Negative change in the normalised difference vegetation index (NDVI) values between post- and pre-cyclone shows damage to vegetation and cropland (Hu & Smith, 2018). Also, Mandal and Hosaka (2020) analysed the impact of cyclones (1988–2016) on Sunderbans mangrove forests (east coast of India) based on the change in NDVI values using Landsat 5, 7 and 8 images. On the other hand, active remote sensing images of COSMO-SkyMED, TerraSAR-X, RADARSAT-1 and 2, Indian Remote Sensing Satellite RISAT-1 and Sentinel-1 SAR sensor have been utilised to detect flooding in urban as well as in rural areas using appropriate threshold range (Mason et al., 2012; Manjusree et al., 2015; Pulvirenti et al., 2016; Clement et al., 2018; Bhatt et al., 2020).

About 0.5 million of people have been safely evacuated from South 24 Parganas, North 24 Parganas, Purba and Pashchimi Medinipur districts of W.B. before the landfall of the Amphan cyclone at 1730 hrs Indian Standard Time (IST) on May 20, 2020 near the W.B. coast (UNICEF India, 2020). Considering the level of the severity of the Amphan cyclone, the present study aims to analyse the impacts of the cyclone on LULC (built-up area, cropland, brick-kiln industries and vegetation cover) of nine districts of W.B. namely, Bardhaman, Nadia,

North 24 Parganas, South 24 Parganas, Purba Medinipur, Paschim Medinipur, Haora and Kolkata.

Study area

The present study has been carried out in W.B. that extends from 86° 47' 34.605" E to 88° 59' 29.06" E longitude and from 21° 33' 50.591" N to 24° 05' 42.42" N latitude and covers 43,887 km² of area. The selection of the study area is based on the track of the Amphan cyclone, wind speed and amount of rainfall over the districts of W.B. (Fig. 1). In the study area, the elevation is ranging from -14 to 477 m above mean sea level (amsl) while the mean elevation is 24 m. The mean slope of the study area is 0.6°. The study area lies in the lower Gangetic plain region where the major geomorphic landforms are formed by the denudation, fluvial and coastal processes (GSI & NRSC, 2012). Hot and sub-humid monsoonal climate prevails in the study area, receiving 80% of the total annual rainfall during monsoon. Average maximum temperature in the summer season ranges from 29 to 33 °C while the average winter temperate varies between 17 and 24 °C (Singh et al., 1998). According to W.B. Disaster Management and Civil Defence Department (WBDM-CDD, 2021) coastal districts of W.B. (North and South 24 Parganas, Purba and Paschim Medinipur) are highly vulnerable to the tropical cyclone originated from the Bay of Bengal. A super cyclone occurred during October 7–12, 1737, over Sunderbans (South 24 Parganas) and caused a surge height of 12 m and a loss of 0.3 million human lives (WBDM-CDD, 2021). During October 2–5, 1864, a cyclone made landfall near Contai (Purba Medinipur) with a storm surge height of 9 m and killed 0.05 million people due to drowning (WBDM-CDD, 2021). Moreover, the landfall of a severe cyclonic storm occurred near Contai again with a storm surge height of 3-5 m and 0.019 million people died during October 14–16, 1942 (WBDM-CDD, 2021).

Amphan cyclone

Wind speed was ranging between 155 and 165 km hr⁻¹ gusting to 185 km hr⁻¹ during the landfall of Amphan cyclone near the W.B. coast on May 20, 2020, at 1730 hrs of IST (IMD, 2020). On the basis of such a high speed, the Amphan cyclone was classified as a very severe cyclonic storm on May 20, 2020. Over W.B.,

Amphan remained as a very severe cyclonic storm (RSMC, 2020). At the time of landfall, the strong winds produced a storm surge of 4.6 m (RSMC, 2020). Further, at 2330 hrs of IST on May 20, 2020, the severe cyclonic storm Amphan was located over Bangladesh (IMD, 2020). Further, on May 21, 2020, at 0830 hours, the cyclone moved north-northeast direction and classified as a cyclonic storm (RSMC, 2020). Thus, the intensity of the Amphan cyclone decreased after the 15 hrs of landfall.

Materials and methods

District and block-wise boundaries have been digitised from the administrative atlas of W.B. (Census of India, 2011a). Gridded rainfall data at 0.25°×0.25° spatial resolution have been obtained from the India Meteorological Department (IMD) to analyse district-wise mean rainfall patterns during May 20–23, 2020 (Pai et al., 2014). Amphan cyclone track has been prepared using all India weather summary dated May 21, 2020 (IMD, 2020; RSMC, 2020). Sentinel-2 is a multispectral instrument (MSI) and consisting of a two-satellite constellation, namely, Sentinel-2A and Sentinel-2B (ESA, 2020a). Sentinel-2 operates in visible, near-infrared and shortwave infrared part of the electromagnetic spectrum (ESA, 2020b). In this study, Sentinel-2B MSI images of pre (May 14, 2020)—and post (June 3, 2020)—cyclonic event have been utilized. Land use and land cover (LULC) mapping and NDVI computation of the study area have been done using Sentinel-2B MSI images of May 14, 2020 while the same sensor images of June 03, 2020 have been used for post-cyclonic event NDVI computation in the Sentinel Application Platform (SNAP) tool. The formula used for the NDVI computation is given in Eq. 1.

$$NDVI = \frac{(Band8 - Band4)}{(Band8 + Band4)} \tag{1}$$

Percentage change in cloud-free districts (North and South 24 Parganas, Paschim Medinipur, Bardhaman, Haora, Kolkata, Hugli and Nadia) of the study area has been analysed using Eq. 2.

$$\% \text{ change in NDVI} = \frac{[(NDVI_{Post-Cyclone} - NDVI_{Pre-Cyclone}) / (NDVI_{Pre-Cyclone})] \times 100}{\tag{2}}$$

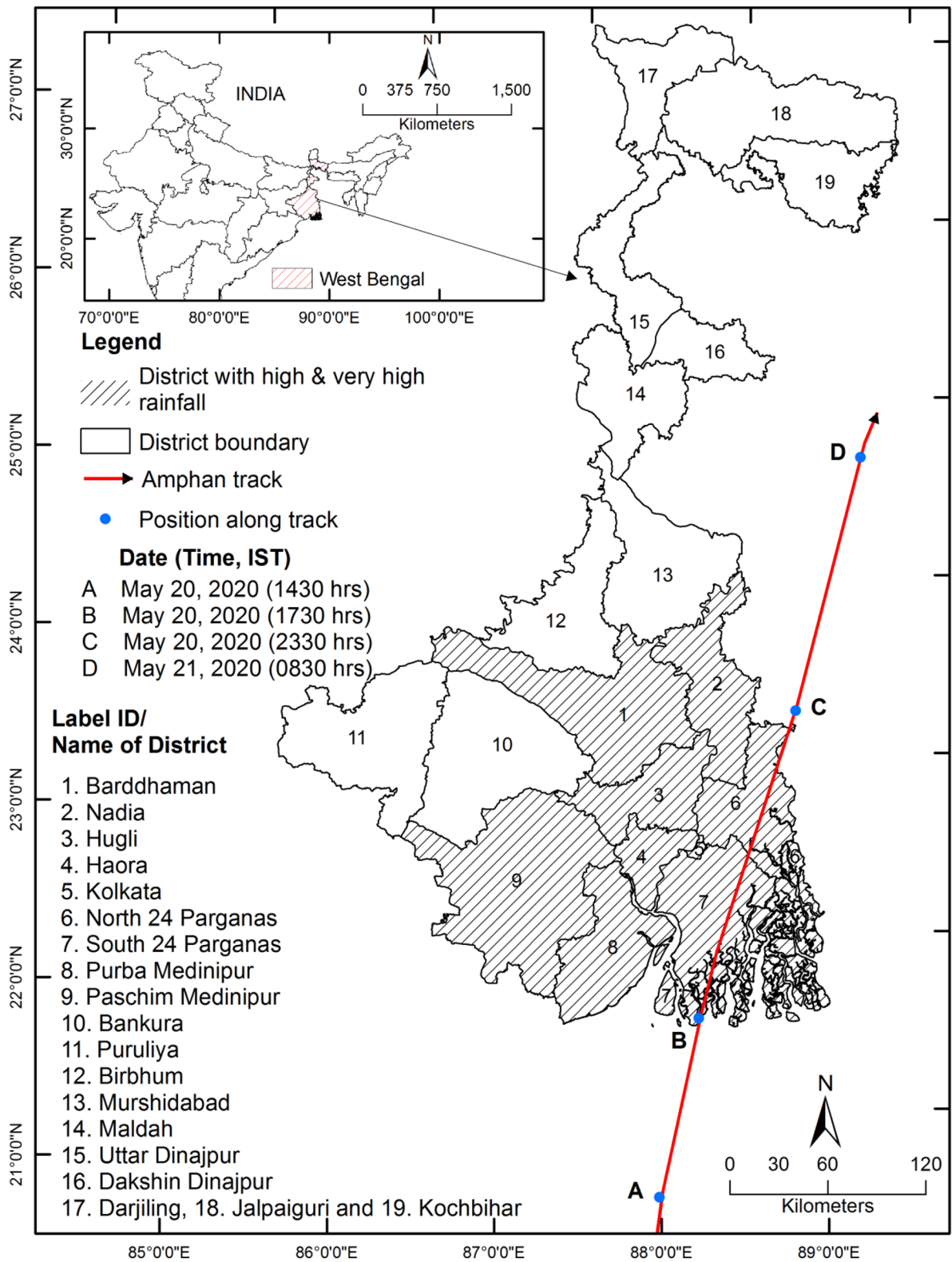


Fig. 1 Location map of the study area

The maximum likelihood classification algorithm of supervised classification has been used for the classification of May 14, 2020, image into six LULC classes, namely, brick-kiln, built-up, cropland, sand, vegetation cover and water body at 10 m spatial resolution. Brick-kilns are considered as a separate land use class because these are important rural industries in the study area. Water body class of May 14, 2020, has been used as pre-cyclone water bodies.

Satellite images from both the active and passive remote sensing platforms are being used for mapping the flooded areas at different spatial scales (Bhatt et al., 2016). Passive or optical remote sensing images can not be used for flooded areas mapping under cloud cover because the passive sensor normally works in visible, near and short wave infrared of the electromagnetic spectrum which is not able to penetrate through the clouds (Ban et al., 2017). Passive sensor devices utilize reflected solar energy for detecting the Earth’s surface features and hence, only work during the day time. Beside this, the synthetic aperture radar (SAR) is an active sensor that has ability to map the flooded areas under cloud cover because it utilizes its own energy in microwave region of the electromagnetic spectrum that can penetrate through the clouds and can work during day and night (Bhatt et al., 2020). Hence, active sensor images are being used extensively for mapping the flooded areas.

Sentinel-1 consists of Sentinel-1A and Sentinel-1B satellite constellation. Sentinel-1 SAR operates at a frequency of 5.405 GHz for the detection of the Earth’s features (ESA, 2020c). This study has utilized Sentinel-1 A and B interferometric wide swath (IW) ground range

detected (GRD) data having dual-polarisation, i.e. VV and VH (Table 1). Processing of the Sentinel-1A and B IW GRD products has been done using SNAP tool. Correction of orbit file, removal of thermal noise, calibration, 7×7 Gamma MAP speckle filtering and Doppler range terrain correction using the Shuttle Radar Topography Mission (SRTM)-1 sec HGT are the standard procedures applied on the VV and VH polarisation images of Sentinel-1A and B IW GRD to obtain geometrically corrected images and backscattering values (σ_0) at 10 m special resolution (Twele et al., 2016). In addition, the conversion of σ_0 values into a logarithmic scale has provided values in decibel (dB). The VV polarization images of Sentinel-1A-B SAR data have been widely used for flooded area detection.

There are generally two methods for flooded-pixels detection from the SAR images, namely, (a) traditional and (b) manually and automatic threshold-based approach. Traditional methods include ground-based survey techniques and mapping of flooded areas and on-screen digitisation of flooded pixels in the GIS environment (Manavalan, 2017). These traditional methods are labour-intensive as well as time-consuming. Contrary to this, manual and automatic training site-based threshold techniques provide quick, accurate and effective flooded area extraction using Sentinel-1 SAR images (Agnihotri et al., 2019; Tiwari et al., 2020). This technique requires more computational power than the traditional technique and is easy to follow.

The VV polarisation images of May 22, 2020, have been used for the flooded area extraction with the help of defined threshold values in dB (Table 1). The flooded-pixels in the VV polarisation SAR image appear dark due to low backscattering. Therefore, well-distributed training sites have been made manually

Table 1 Description of Sentinel-1A SAR data

Scene ID	Date of acquisition	Track	Orbit	Water threshold range (dB) for VV polarization
S1A_IW_GRDH_1SDV_20200522T000419_20200522T000444_032_670_03C8AC_635E	22-05-2020	48	32,670	−27.5008 to −14.4755
S1A_IW_GRDH_1SDV_20200522T000444_20200522T000509_032_670_03C8AC_A6E3	22-05-2020	48	32,670	−33.8188 to −19.5408
S1B_IW_GRDH_1SDV_20200522T235525_20200522T235550_021_701_029311_859D	22-05-2020	150	21,701	−30.5966 to −15.9867
S1B_IW_GRDH_1SDV_20200522T235550_20200522T235615_021_701_029311_F87B	22-05-2020	150	21,701	−33.2898 to −14.6681

on the flooded-pixels of different images of Sentinel-1A-B using SNAP tool. Statistics of all training site of a particular scene has been used to prepare a histogram (UN-SPIDER Knowledge Portal, 2021). Further, minimum and maximum backscattering values (threshold range) have been selected with the help of histogram statistics to separate flooded pixels (Table 1).

Due to non-availability of Sentinel-2 MSI images, resampling of the flooded and non-flooded areas extracted from Sentinel-1 images has been done at 15 m spatial resolution for accuracy assessment with the help of the Landsat 8 Pan band of 15 m spatial resolution. Accuracy of the flooded and non-flooded areas has been done using an error matrix that is constructed with the help of a sum of 111 random reference points for flooded and non-flooded areas, created on the Landsat 8 Operational Land Imager (OLI)-Thermal Infrared Sensor (TIRS) (Path-138 and row- 44 and 45) dated May 24, 2020 (Table 2). However, the LULC accuracy has been carried out by taking a sum of 180 random reference points for different classes from the Google Earth image (Table 3).

Actual flooded area has been computed by the subtraction of pre-cyclone water bodies (May 14, 2020) from the total flooded areas (May 22, 2020). Overlay analysis has been performed using the actual flooded area and LULC to obtain the flood-affected LULC in the study area. SRTM digital elevation model (DEM) at 30 m spatial resolution has been used for the computation of mean elevation of the district and actual flooded areas. A flowchart of methods used in this study has been given in Fig. 2.

Results and discussion

Rainfall pattern over West Bengal

IMD records rainfall at 0830 hrs of IST every day. Before landfall, the mean rainfall over the study area is ranging between 5.5 and 31.7 mm

Table 2 Accuracy assessment of non-flooded and flooded areas

Class	Producer's accuracy (%)	Omission error (%)	User's accuracy (%)	Commission error (%)
Non-flooded	94.83	5.17	90.16	9.84
Flooded	88.68	11.32	94	6

Overall accuracy = 92%; kappa coefficient = 0.8371

Table 3 Accuracy assessment of LULC classes

Class	Producer's accuracy (%)	Omission error (%)	User's accuracy (%)	Commission error (%)
Built-up	100.0	0.0	100.0	0.0
Cropland	90.9	9.1	72.3	27.7
Vegetation	50.0	50.0	72.2	27.8
Water bodies	87.5	12.5	87.5	12.5
Brick-klin	81.5	18.5	100.0	0.0
Sand	88.6	11.4	100.0	0.0

Overall accuracy = 84%; kappa coefficient = 0.79

from May 19 (0830 hrs onwards) to May 20 (up to 0830 hrs) (Fig. 3a). After the landfall, the movement of Amphan across the study area caused torrential rainfall. Consequently, mean rainfall over the study area is varying from 48.6 to 235.9 mm during May 20 (0830 hrs onwards)-May21 (up to 0830 hrs) (Fig. 3b). On May 22 and 23, 2020, the study area received less rainfall compared to the northern districts of W.B. because of the movement of the cyclonic storm further north-northeast part of Bangladesh (Fig. 3c, d).

LULC of the study area

Pre-cyclone mapping of LULC categories is necessary for the estimation of cyclone-induced damage (Hoque et al., 2016). The LULC classification results illustrate that cropland, vegetation cover, built-up, water body, sand and brick-kiln industry classes cover 65.8, 20.7, 8.2, 4.9, 0.2 and 0.1% of the total study area, respectively (Fig. 4). The overall accuracy of LULC classes is 84% with a kappa coefficient of 0.79.

Actual flooded area

Total actual flooded area is 488 km² which accounts for only 1% area of the total study area on May 22, 2020. The overall accuracy of flooded and non-flooded areas is 92% with a kappa coefficient of 0.84. In terms of percentage to the total actual flooded area, Purba Medinipur has the largest share (22%) followed by Bardhaman, North 24 Parganas, Hugli, Nadia, Paschim Medinipur, South 24 Parganas, Haora and Kolkata (Table 4). Flooding and waterlogging in

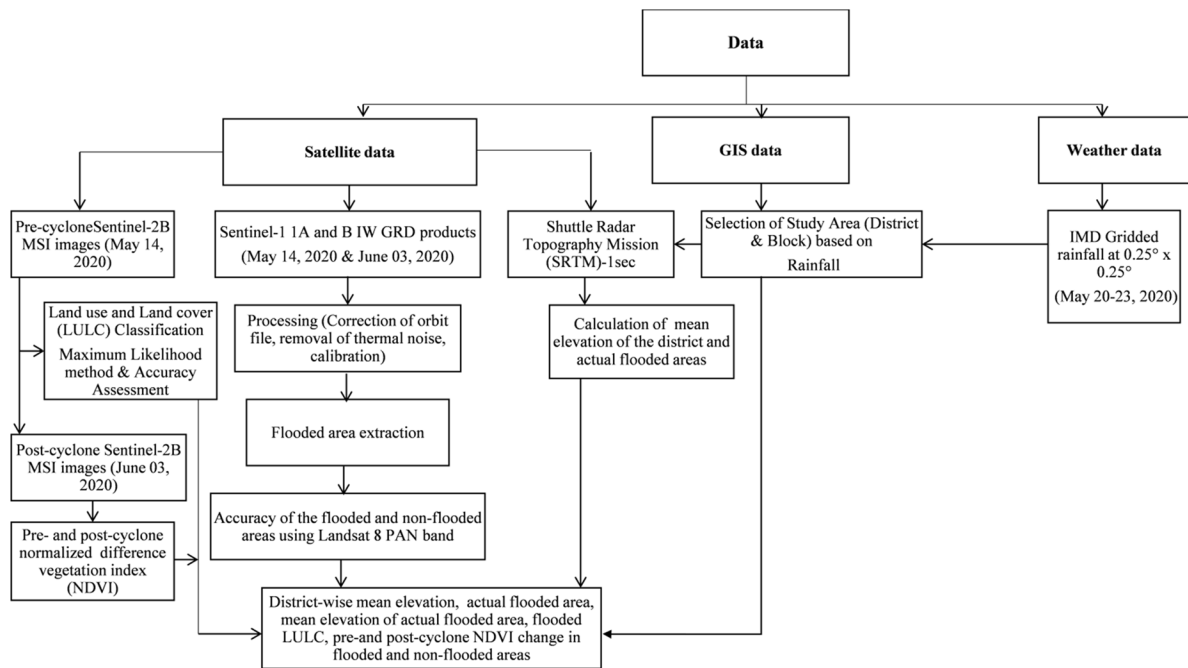


Fig. 2 Methodology of data processing of the study area

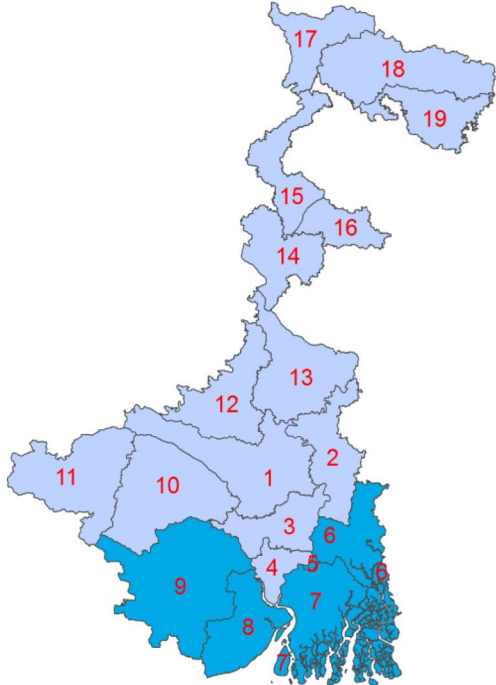
southern and eastern parts of Purba Medinipur, southern parts of South 24 Parganas and North 24 Parganas districts are mainly caused by the storm surge (Fig. 5). However, flooding and waterlogging in Bardhaman, Nadia, Haora, Hugli, Paschim Medinipur, central and northern parts of North 24 Parganas, the western part of Purba Medinipur and northern and western parts of South 24 Parganas are caused by the torrential rainfall. Kolkata airport located in North 24 Parganas district is flooded and well-sensed by the Sentinel-1A and B IW GRD SAR. However, in Kolkata metropolitan areas, waterlogging and flooded areas have not been detected like the rural areas by the Sentinel-1A and B IW GRD SAR due to moderate spatial resolution. The mean elevation of actual flooded areas is lower than the mean elevation of each district, indicating that low-lying areas are flooded (Table 4).

Flood-affected LULC

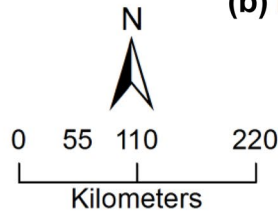
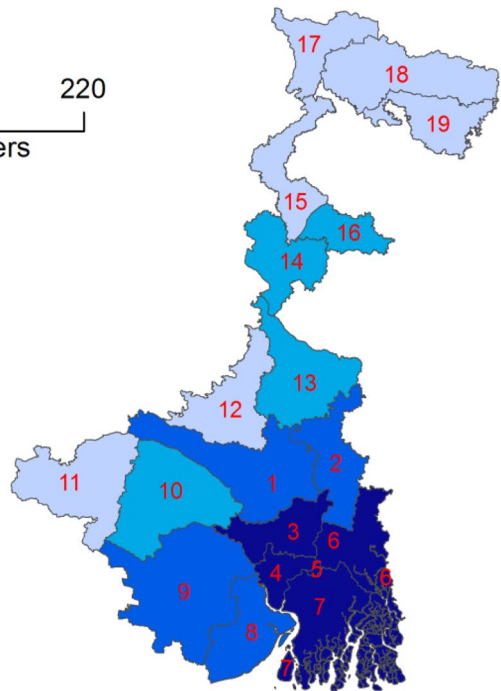
Cropland covers large chunk (88.2%) of the total actual flooded areas (488 km²), followed by sand (4.9%), vegetation cover (4.4%), built-up (2.1%) and brick-kiln (0.4%). Purba Medinipur accounts for 24% of the total

flood-affected cropland (430.43 km²), followed by North 24 Parganas (16%), Barddhaman (15%), Hugli (13%), Nadia (12%), South 24 Parganas (7%), Paschim Medinipur (7%) and Haora (5%). Boro paddy, betel vine, summer vegetables, green gram and sesame crops have been damaged in Purba Medinipur and South 24 Parganas (GKMS & IMD, 2020). Storm-surge-induced flooding in southern parts of Purba Medinipur, South 24 Parganas and North 24 Parganas districts may increase the salinity of cropland due to intrusion of seawater and consequently, soil fertility would reduce (Samanta, 1997). The total flood-affected area of riverine sand is 24.14 km² out of which 55% area lies in Barddhaman and the remaining in Paschim Medinipur. Torrential rainfall caused lateral expansion of the river and as a consequence, sandy point and lateral bars get inundated in Barddhaman and Paschim Medinipur district. Such inundation affects sand mining activities in these districts. The flood-affected vegetation cover area accounts for 21.26 km². North 24 Parganas covers large chunk (22%) of the affected vegetation areas, followed by South 24 Parganas (17%), Hugli (16%), Purba Medinipur (12%), Haora (12%), Barddhaman (8%), Nadia (7%), Paschim Medinipur (6%) and Kolkata (0.1%) district. In the study area, the total flood-affected

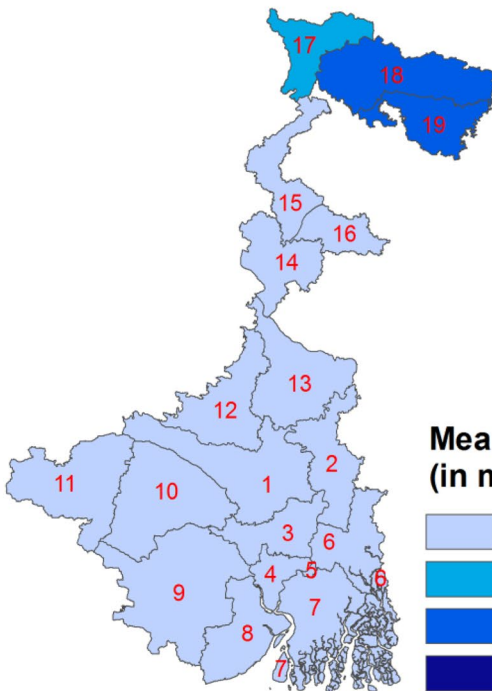
(a) May 20, 2020



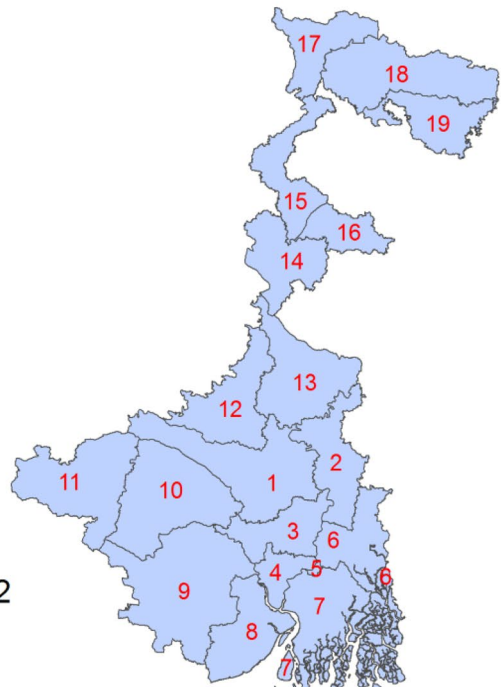
(b) May 21, 2020



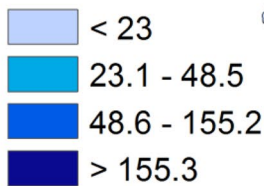
(c) May 22, 2020



(d) May 23, 2020



**Mean rainfall
(in mm)**



◀ **Fig. 3** District-wise distribution of cyclonic rainfall (in mm) during May 20–23, 2020

built-up area is 10.18 km². North 24 Parganas covers about 41% of the total affected built-up areas, followed by Nadia (21%), Barddhaman (17%), South 24 Parganas (14%), Hugli (4%), Paschim Medinipur (2%), Haora (1%) and Kolkata (0.1%) districts. Overall flood-affected built-up areas in these districts are located in low lying areas. In addition, the visual interpretation of flooded area and built-up area layers shows that most of the built-up areas are marooned in Purba Medinipur district. The total flooded brick-kiln area is 2.04 km² out of which 76% of the area lies in North 24 Parganas and the remaining 24% area is in Purba Medinipur district. In these districts, the brick-kiln industries are located near to the waterbodies. Furthermore, torrential rainfall increases the water level in the water bodies as a result, brick-kiln industries get flooded.

Impact of Amphan cyclone on NDVI values of cropland and vegetation cover

Reduction in NDVI values denotes loss of crops or vegetation cover while an increase in NDVI values reflects healthy crops and vegetation cover (Kumar, 2016). High-speed winds and torrential rainfall cause damage to vegetation cover and standing crops. Furthermore, defoliation and uprooted trees due to strong winds cause reduction in NDVI values (Walcker et al., 2019; Lin et al., 2020). In flood and cyclone impact-related studies, reduction in NDVI values has been taken as proxy to damage (Tehrany et al., 2015; Kumar, 2016; Hu & Smith, 2018; Dodangeh et al., 2020). NDVI change analysis has been done only for the cloud-free part covering 29% of the total study area. These days, drone and Unmanned Aerial Vehicle (UAV)-based survey techniques are the best alternatives to capture damage to built-up, cropland

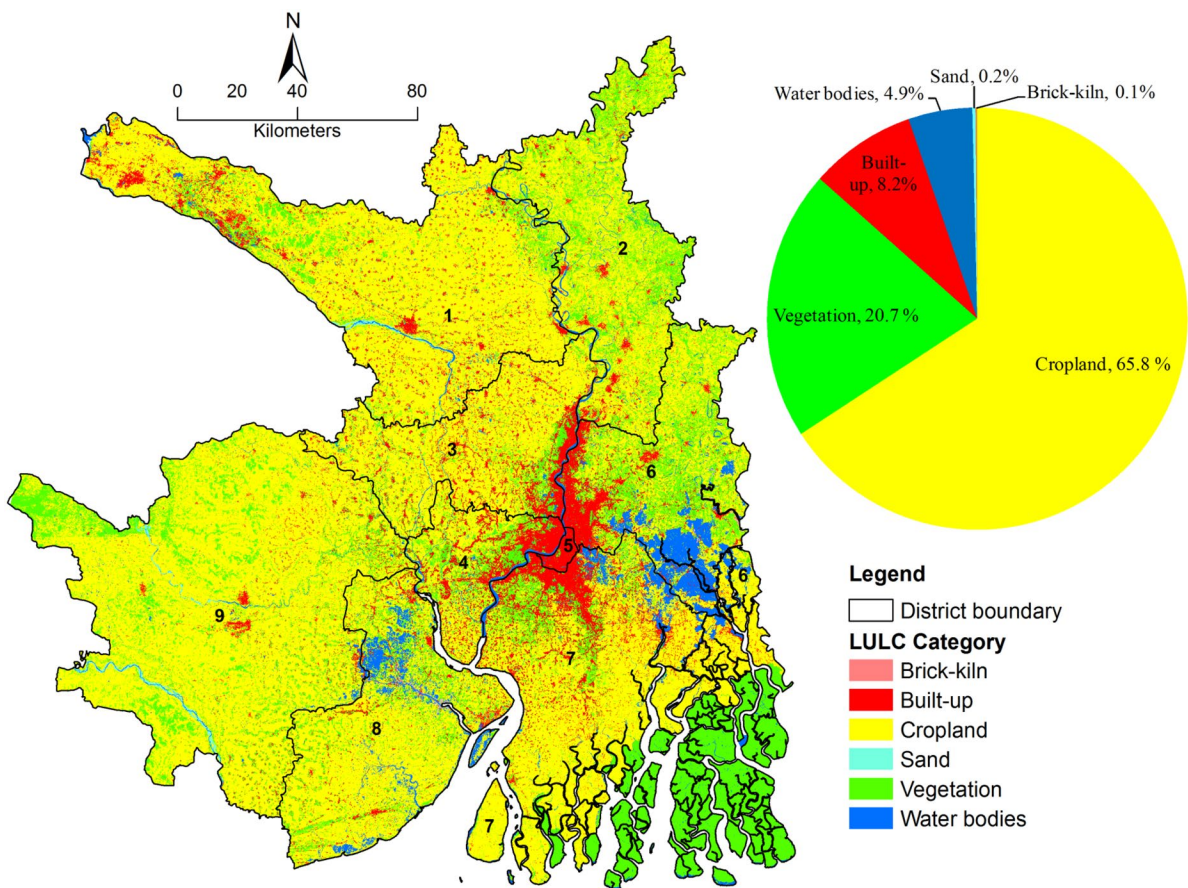


Fig. 4 Distribution of LULC in the study area before the cyclone (May 14, 2020)

Table 4 District-wise mean elevation, district area, actual flooded areas, mean elevation of actual flooded area, percentage to the total actual flooded area and percentage of actual flooded area to district area on May 22, 2020

Label ID	District name	Mean elevation of district (m, amsl)	District area* (km ²)	Actual flooded area (km ²)	Mean elevation of actual flooded area (m, amsl)	Percentage to the total actual flooded area	Percentage of actual flooded area to district area
1	Bardhaman	46	7024	82.7	30	17	1.2
2	Nadia	14	3927	54.2	12	11	1.4
3	Hugli	14	3149	61.6	11	13	2.0
4	Haora	8	1467	24.3	7	5	1.7
5	Kolkata	10	185	0.03	8	0	0.0
6	North 24 Parganas	8	4094	81.5	7	17	2.0
7	South 24 Parganas	5	9960	36.8	4	8	0.4
8	Purba Medinipur	6	4713	105.9	5	22	2.2
9	Paschim Medinipur	48	9368	41.2	19	8	0.4
Total			43,887	488		100	1.1

*Source: Census of India (2011b)

and vegetation cover if the area is under cloud cover (Greenwood et al., 2020; Schaefer et al., 2020).

On May 14, 2020, overall mean NDVI of the non-flooded cropland in the selected cloud-free part is 0.58 ± 0.22 and it reduced to 0.56 ± 0.22 on June 3, 2020. Mean NDVI of vegetation cover is 0.71 ± 0.15 on May 14, 2020, and it further reduced to 0.68 ± 0.19 on June 3, 2020. Overall mean NDVI values of non-flooded cropland and vegetation cover have been reduced by 3.4 and 4%, respectively. Overall mean NDVI values of flood-affected cropland and vegetation cover are 0.34 ± 0.15 and 0.60 ± 0.19 on May 14, 2020 while it reduced to 0.27 ± 0.25 and 0.38 ± 0.34 on June 3, 2020, respectively. Furthermore, mean NDVI values of flood-affected cropland and vegetation cover have been reduced by 21 and 37%, respectively, between May 14, 2020 and June 3, 2020.

Pixel-wise analysis for change in NDVI values in the non-flooded cropland areas shows that the areal coverage of improvement in NDVI values is higher than the reduction. However, non-flooded vegetation cover area shows that the areal coverage of reduction in NDVI values is more than the improvement in NDVI values. On the other hand, flooded cropland and vegetation cover collectively show that the areal coverage of reduction in NDVI values is higher than the improvement in NDVI values (Table 5) (Figs. 6, 7 and 8).

District level NDVI change analysis for non-flooded cropland shows that Hugli records high reduction

(9.8%) in NDVI values, followed by Bardhaman, Paschim Medinipur, Haora, North 24 Parganas and South 24 Parganas (Table 6a) while Nadia district is showing an improvement in NDVI values. For non-flooded vegetation cover, North 24 Parganas district shows the highest reduction in NDVI values, followed by South 24 Parganas, Paschim Medinipur, Hugli, Bardhaman, Kolkata and Haora (Table 6b). However, Nadia district is showing an improvement in NDVI values in non-flooded vegetation cover. The highest reduction in NDVI values of flood-affected cropland has been observed in North 24 Parganas while the lowest in Hugli district (Table 6c). However, the reduction in NDVI values for flooded-affected vegetation cover is highest in Nadia and lowest in Paschim Medinipur district (Table 6d). Reduction in NDVI values for cropland and vegetation cover shows inter-district variations. State Inter Agency Group (2020) has also listed out that Kolkata, South and North 24 Parganas, Purba and Paschim Medinipur, Haora, and Hugli districts are severely affected by the cyclone while Nadia and Bardhaman districts are relatively less affected.

Block-wise analysis of flooded cropland indicates a reduction in NDVI values in about 88% of the total blocks (97) which are showing the scale of impact of the cyclone (Table 7). The highest reduction (-204.9%) in NDVI of the flooded cropland has been observed in Garbeta-I block of Paschim Medinipur district while the lowest reduction (-1.5%) has been found in Rajarhat

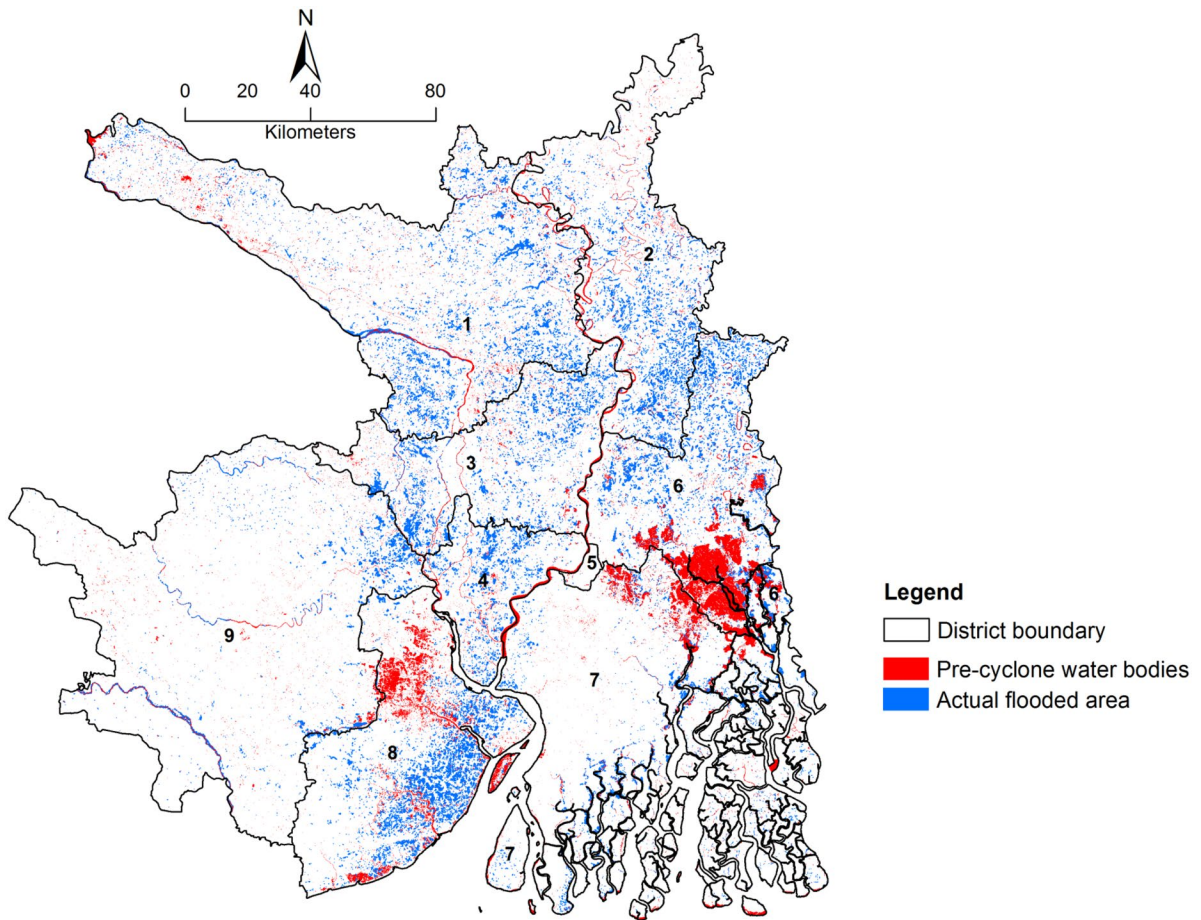


Fig. 5 Pre-cyclone water bodies and post-cyclone actual flooded area on May 22, 2020

block of North 24 Parganas district (Fig. 9a). However, 22% of blocks have shown improvement in NDVI which varied from 0.2% (Bagda block of North 24 Parganas) to 55.7% (Keshpur block of Paschim Medinipur district) indicating that the flooded croplands have not been substantially damaged by the cyclone. The areas of Keshpur block are extensively utilized for the cultivation of paddy and vegetables (Akram et al., 2019) and an improvement in NDVI values is indicating less impact of the cyclone on cropland in this block (Fig. 9a).

In the case of the non-flooded cropland, about 69% of the total blocks (99) show a reduction while 31% of blocks have shown improvement in NDVI values (Table 8). The highest reduction (−28.4%) in the non-flooded cropland has been observed in Basirhat-I block of North 24 Parganas while the lowest (−0.3%) has been found in Magrahat-II of South 24 Parganas

district (Fig. 9b). Besides this, an improvement in NDVI values, indicating healthy cropland in some blocks of W.B., ranges between 0.1(Barrackpur-I block of North 24 Parganas) and 13.4% (Karimpur-I block of Nadia district). Some blocks have shown a negligible change in NDVI during the cyclonic event (e.g. Jagatballavpur, Barrackpur-I, Bishnupur-II and Barasat-II) (Fig. 9b).

In the context of flooded vegetation, 92% of the total blocks (93) are showing a reduction in NDVI while only 8% of blocks are showing improvement (Table 9). The highest reduction (−107%) has been seen in De-ganga block of North 24 Parganas district while the lowest reduction (−1.5%) is in Burdwan-I block of Barddhaman district (Fig. 10a). Besides this, an improvement in NDVI values is varying from 2.3% (Pandua block of the Hugli district) to 15% (Khanakul-I block of Hugli

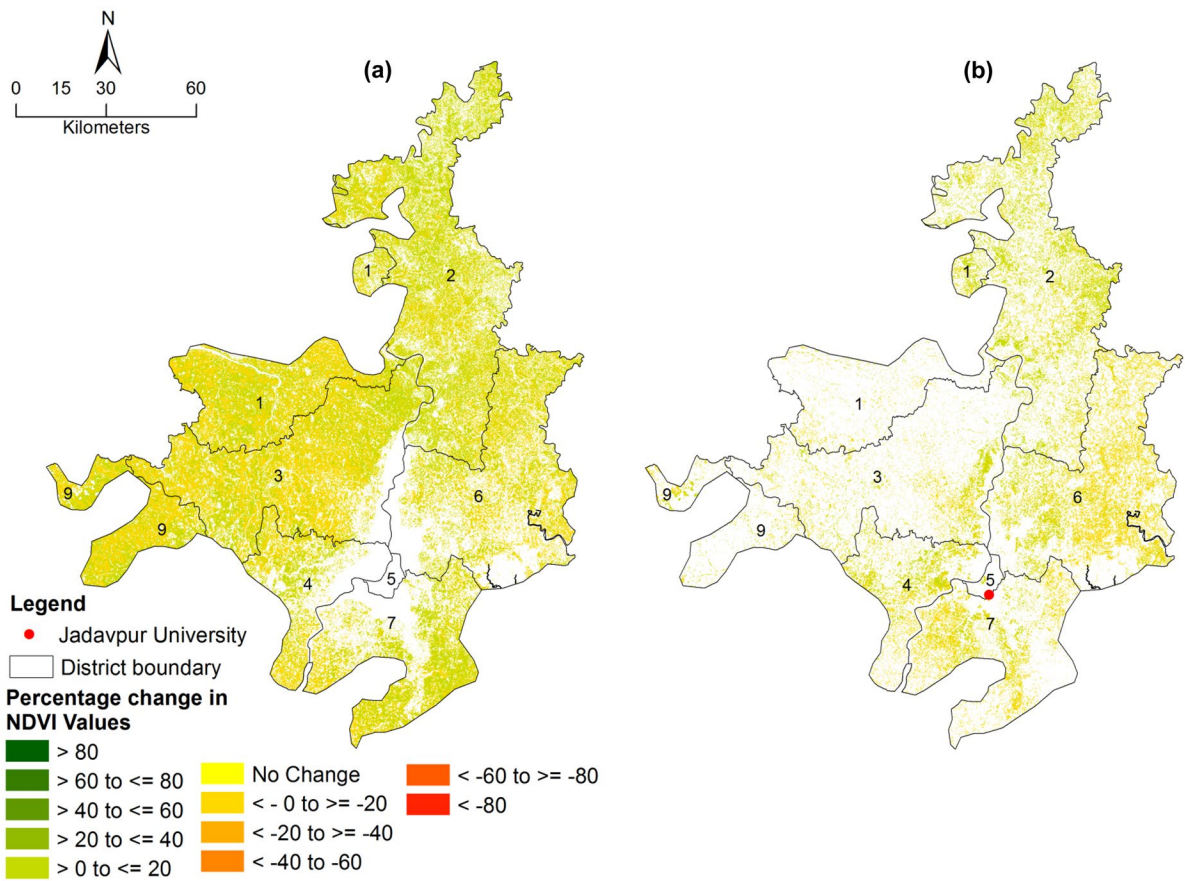


Fig. 6 Pixel-wise percentage change in NDVI values in the non-flooded (a) cropland and (b) vegetation cover

district) and is indicating no substantial effect of flooding on vegetation cover in some of the blocks (Table 9).

In the case of the non-flooded vegetation cover, 75% of total blocks are showing a reduction in the NDVI while only 25% of blocks are denoting healthier vegetation cover in the post-cyclone period than that in the pre-cyclone period (Table 10). Further, the highest reduction (−19.9%) of the NDVI values in the non-flooded vegetation cover has been seen in Basirhat-II block of North 24 Parganas district possibly due to high-speed winds during the cyclone movement while Chinsurah block of Hugli shown lowest reduction (−0.1%) in NDVI. The improvement in NDVI is ranging from 0.4% (Sonarpur block of South 24 Parganas district) to 5.9% (Tehatta-II block of Nadia district). Ranaghat-I, Krishnaganj, Krishnaganj-II, Kaliganj, ChapraNakashipara, Tehatta, Karipur-II and

Tehatta-II blocks, located in the northern part of Nadia district, are showing an improvement in NDVI due to weak wind speed (Fig. 10b).

Pixel, district and block-wise variations in changes in NDVI values has been observed in both the flooded and non-flooded cropland and vegetation cover indicating the differences in the impacts of the cyclone. It might be occurred due to species diversity and the growth level of crops and vegetation. The study emphasises the need for further investigations in this context to understand the impact of the cyclone on different crops and vegetation species to minimise its impacts in the future. It also helps the planners to select crop and vegetation species in highly vulnerable areas of W.B. which can adjust to high-speed winds and flooding. It would be useful for the livelihood sustainability of the cyclone prone areas.



Fig. 7 Uprooted trees in the non-flooded Jadavpur university (main campus), Kolkata. The reduction in NDVI values in the campus is ranging from < -0 to ≥ -20

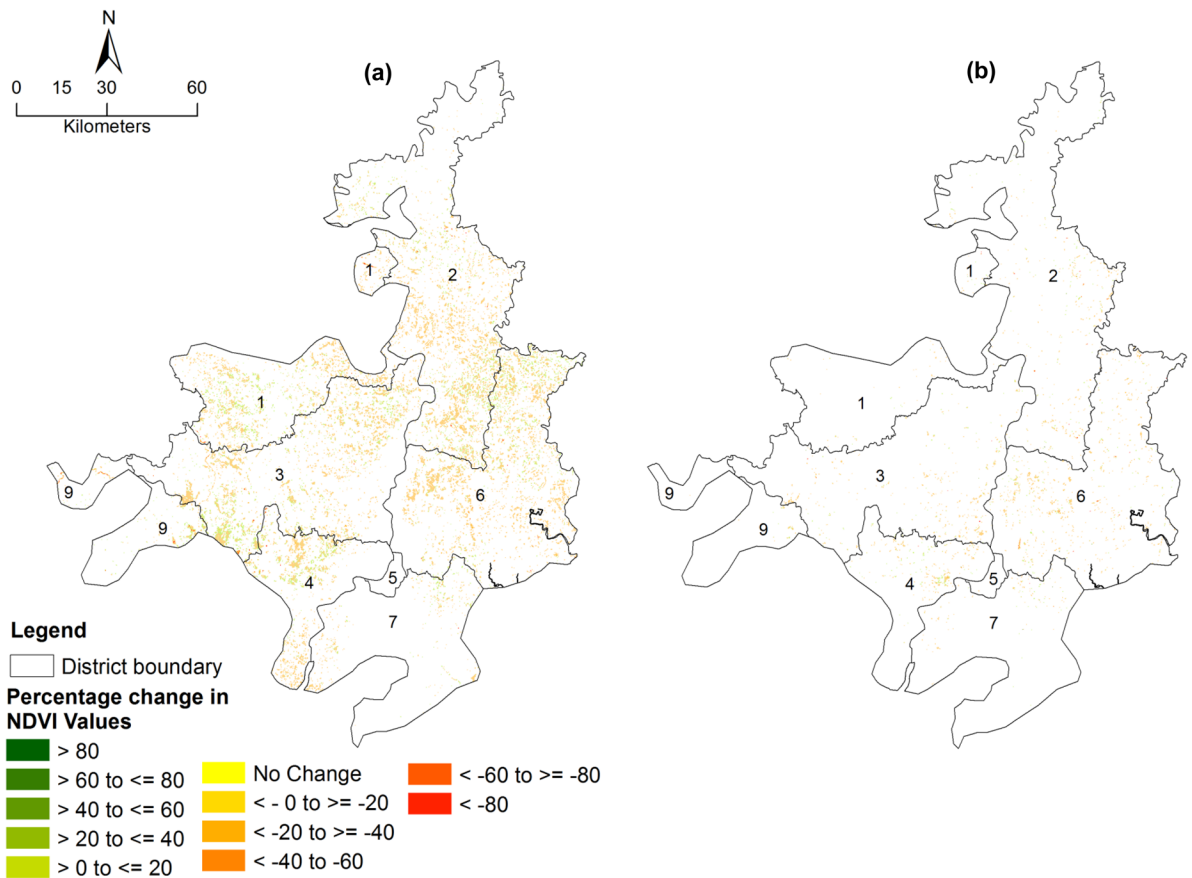


Fig. 8 Pixel-wise percentage change in NDVI values in the flood-affected (a) cropland and (b) vegetation cover

Table 5 Percentage change in NDVI values for flood-affected and non-flooded cropland and vegetation cover

Change in NDVI (in %)	Flood-affected area (km ²)		Non-flooded area (km ²)	
	Cropland	Vegetation	Cropland	Vegetation
> 80	0.03	0.0024	0.2	0.1
> 60 to ≤ 80	0.01	0.0007	0.1	0.0
> 40 to ≤ 60	0.02	0.0015	0.2	0.1
> 20 to ≤ 40	0.07	0.0052	0.5	0.2
> 0 to ≤ 20	90.40	3.7414	4670.4	1593.4
No change	0.00	0.0004	0.0	0.0
< -0 to ≥ -20	119.75	8.8384	4438.3	1640.0
< -20 to ≥ -40	0.09	0.0050	0.5	0.2
< -40 to -60	0.02	0.0015	0.2	0.1
< -60 to ≥ 80	0.01	0.0008	0.1	0.0
< -80	0.04	0.0026	0.3	0.1
Total	210.46	12.60	9110.77	3234.03

Table 6 District-wise mean, standard deviation (SD) and percentage change in NDVI of the study area

District	May 14, 2020		June 3, 2020		% Change
	Mean	SD	Mean	SD	
(a) Mean NDVI change in non-flooded cropland					
Hugli	0.61	0.23	0.55	0.22	-9.8
Barddhaman	0.54	0.23	0.51	0.22	-7.1
Paschim Medinipur	0.65	0.23	0.60	0.20	-7.0
Haora	0.57	0.21	0.53	0.22	-6.7
North 24 Parganas	0.57	0.20	0.54	0.23	-6.4
South 24 Parganas	0.53	0.17	0.51	0.16	-4.2
Nadia	0.59	0.21	0.61	0.22	3.0
(b) Mean NDVI change in non-flooded vegetation cover					
North 24 Parganas	0.70	0.15	0.63	0.20	-10.0
South 24 Parganas	0.69	0.14	0.64	0.16	-7.7
Paschim Medinipur	0.74	0.15	0.71	0.19	-4.8
Hugli	0.71	0.16	0.68	0.20	-4.1
Barddhaman	0.71	0.14	0.68	0.20	-3.7
Kolkata	0.71	0.16	0.69	0.18	-2.8
Haora	0.70	0.15	0.69	0.18	1.5
Nadia	0.71	0.14	0.72	0.17	-1.8
(c) Mean NDVI change in flood-affected cropland					
North 24 Parganas	0.31	0.13	0.19	0.22	-39.1
Nadia	0.32	0.12	0.22	0.22	-32.0
South 24 Parganas	0.40	0.19	0.32	0.23	-21.6
Barddhaman	0.33	0.15	0.28	0.23	-15.1
Haora	0.40	0.16	0.37	0.20	-9.1
Paschim Medinipur	0.29	0.25	0.26	0.47	-8.6
Hugli	0.38	0.16	0.35	0.24	-7.1
(d) mean NDVI change in flood-affected vegetation cover					
Nadia	0.59	0.23	0.20	0.36	-65.6

Table 6 (Continued)

District	May 14, 2020		June 3, 2020		% Change
	Mean	SD	Mean	SD	
North 24 Parganas	0.58	0.21	0.32	0.33	-45.6
Hugli	0.63	0.16	0.42	0.35	-33.6
Barddhaman	0.60	0.19	0.45	0.32	-25.6
South 24 Parganas	0.59	0.21	0.45	0.27	-23.7
Haora	0.58	0.16	0.50	0.24	-13.9
Kolkata	0.66	0.18	0.63	0.11	-4.5
Paschim Medinipur	0.63	0.20	0.62	0.23	-2.1

Table 7 Percentage change in NDVI values of flooded cropland of the cloud-free part of the study area

Percentage change in NDVI values	Flooded-cropland District: block name (label ID)	No. of blocks
-204.9 to -110.9 (high)	Paschim Medinipur: Garbeta-I (99), Garbeta-II (103); North 24 Parganas: De-ganga (69), Basirhat-II (64), Basirhat-I (63); Barddhaman: Purbasthali-II (2) & Nadia: Santipur (56)	07
-110.8 to -53.1 (moderate)	Barddhaman: Burdwan-I (5), Burdwan-II (8); Haora: Bally Jagachha (23), Sank-rail (22); Hugli: Serampur Uttarpara (36); Nadia: Krishnagar (53), Krishna-ganj (54); North 24 Parganas: Hasnabad (62), Minakhan (61), Baduria (65), Barasat-II (72), Swarupnagar (66), Barrackpur-II (75) & South 24 Parganas: Bishnupur-I (90)	14
-53 to 0 (low)	Barddhaman: Khandaghosh (3), Memari-II (1), Kalna-II (10), Memari-I (9), Raina-II (4); Haora: Shyampur-I (18), Uluberia-I (19), Shyampur-II (17), Amta-I (15), Jagatballavpur (16), Bagnan-I (14); Hugli: Goghat-II (26), Arambag (30), Goghat-I (27), Singur (37), Haripal (38), Chanditala-I (34), Tarakeswar (33), Pursura (31), Balagarh (41), Chanditala-II (35), Hugli—Chinsurah (25), Pandua (40), Dhaniakhali (39), Chinsurah-Magra (42); Nadia: Ranaghat-I (58), Hanskhali (55), Haringhata (59), Karimpur-II (46), Krishna-gar-II (52), Ranaghat-II (57), Chapra (51), Chakdah (44); North 24 Parganas: Barasat (71), Barrackpur-I (74), Habra-II (70), Amdanga (73), Bongaon (67), Gaighata (76), Habra-I (68), Rajarhat (60); South 24 Parganas: Kulpi (93), Diamond Harbour-II (79), Magrahat-I (91), Budge Budge-II (81), Bishnupur-II (89), Budge Budge-I (82), Sonarpur (84), Baruipur (92), Falta (80), Thakur-pukur Mahestola (83), Jaynagar-I (78), Bhangar-II (85) & Paschim Medinipur: Chandrakona-I (98), Ghatal (102)	55
0.1 to 55.7 (improvement)	Barddhaman: Jamalpur (7), Raina-I (6); Haora: Domjur (11), Uluberia-II (20), Amta-II (12), Panchla (21), Udaynarayanpur (13); Hugli: Jangipara (32), Khanakul-II (28), Khanakul-I (29); Nadia: Nakashipara (50), Karimpur-I (45), Tehatta-II (47), Kaliganj (48), Tehatta-I (49); North 24 Parganas: Bagda (77); South 24 Parganas: Bhangar-I (86), Jaynagar-II (97), Mathurapur-I (96) & Paschim Medinipur: Chandrakona-II (101), Keshpur (100)	21
Total		97

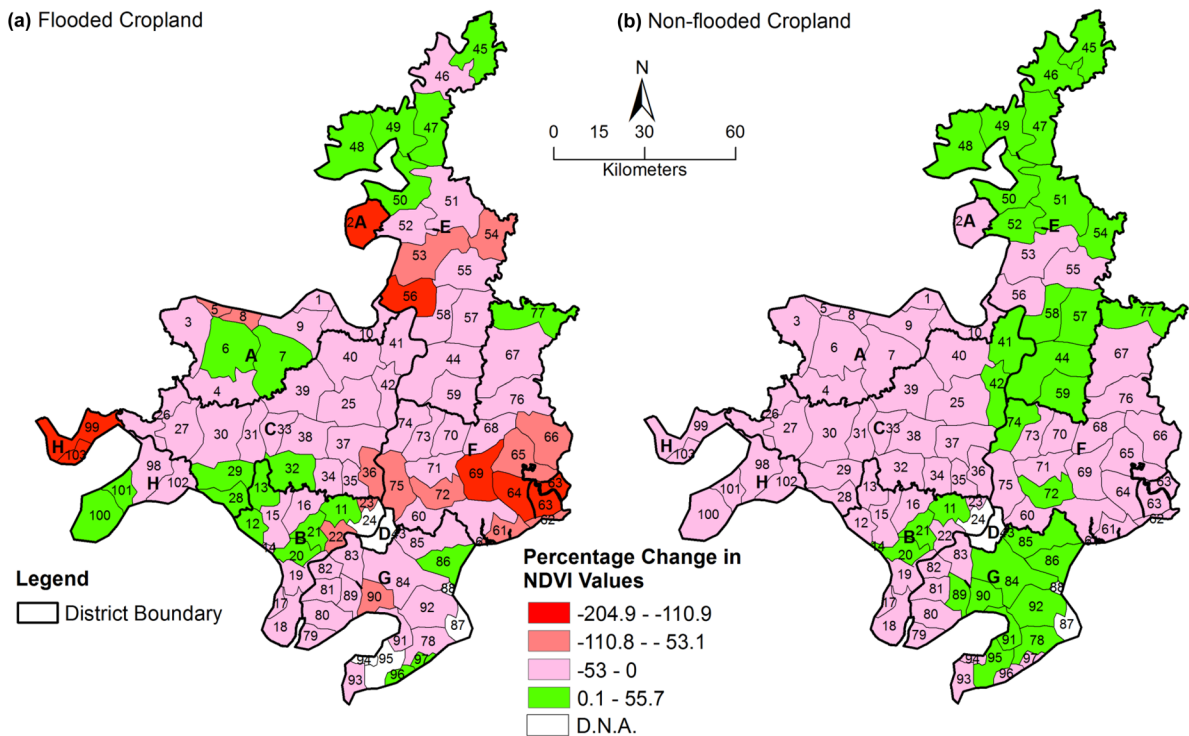


Fig. 9 Block-wise percentage NDVI change in (a) flooded and (b) non-flooded cropland. Label IDs A–H are denoting Bardhaman, Haora, Hugli, Kolkata, Nadia, North 24 Parganas, South 24 Parganas and Paschim Medinipur districts of W.B., respectively

Table 8 Percentage change in NDVI values of non-flooded cropland of the cloud-free part of the study area

Percentage change in NDVI values	Non-flooded-cropland District: block name (label ID)	No. of blocks
-204.9 to -110.9 (high)	N.A	N.A
-110.8 to -53.1 (moderate)	N.A	N.A
-53 to 0 (low)	Bardhaman: Memari-II (1), Khandaghosh (3), Kalna-II (10), Memari-I (9), Raina-II (4), Jamalpur (7), Burdwan-I (5), Burdwan-II (8), Raina-I (6), Purbasthali-II (2); Haora: Shyampur-I (18), Udaynarayanpur (13), Amta-II (12), Shyampur-II (17), Uluberia-I (19), Sankrail (22), Amta-I (15), Bally Jagachha (23), Jagatballavpur (16); Hugli: Chanditala-I (34), Haripal (38), Jangipara (32), Tarakeswar (33), Goghat-I (27), Goghat-II (26), Serampur Uttarpara (36), Arambag (30), Singur (37), Dhaniakhali (39), Pursura (31), Hugli—Chinsurah (25), Khanakul-I (29), Pandua (40), Chanditala-II (35), Khanakul-II (28); Nadia: Krishnagar (53), Hanskhali (55), Santipur (56); North 24 Parganas: Basirhat-I (63), Basirhat-II (64), Minakhan (61), De-ganga (69), Baduria (65), Swarupnagar (66), Habra-I (68), Hasnabad (62), Gaighata (76), Barrackpur-II (75), Habra-II (70), Amdanga (73), Barasat (71), Bongaon (67), Rajarhat (60); South 24 Parganas: Diamond Harbour-II (79), Budge Budge-I (82), Falta (80), Budge Budge-II (81), Kulpi (93), Jaynagar-II (97), Thakurpukur Mahestola (83), Mathurapur-I (96), Magrahat-II (94) & Paschim Medinipur: Chandrakona-I (98), Garbeta-I (99), Chandrakona-II (101), Keshpur (100), Garbeta-II (103), Ghatal (102)	68

Table 8 (Continued)

Percentage change in NDVI values	Non-flooded-cropland District: block name (label ID)	No. of blocks
0.1 to 55.7 (improvement)	Haora: Domjur (11), Uluberia-II (20), Panchla (21), Bagnan-I (14); Hugli: Chinsurah-Magra (42), Balagarh (41); Nadia: Kaliganj (48), Haringhata (59), Krishnaganj (54), Ranaghat-II (57), Nakashipara (50), Chapra (51), Ranaghat-I (58), Chakdah (44), Tehatta-I (49), Krishnagar-II (52), Tehatta-II (47), Karimpur-II (46), Karimpur-I (45); North 24 Parganas: Barrackpur-I (74), Barasat-II (72), Bagda (77) & South 24 Parganas: Bishnupur-II (89), Mandirbazar (95), Jaynagar-I (78), Magrahat-I (91), Bhangar-I (86), Bishnupur-I (90), Bhangar-II (85), Sonarpur (84), Baruiপুর (92)	31
Total		99

Table 9 Percentage change in NDVI values of flooded vegetation cover of the cloud-free part of the study area

Percentage change in NDVI values	Flooded-vegetation cover District: block name (label ID)	No. of blocks
−107.1 to −78.2 (high)	Nadia: Kaliganj (48), Ranaghat-I (58), Santipur (56), Ranaghat-II (57), Krishnaganj (54) and North 24 Parganas: De-ganga (69), Basirhat-I (63), Basirhat-II (64), Baduria (65)	09
−78.1 to −42 (moderate)	Barddhaman: Purbasthali-II (2); Haora: Bally Jagachha (23), Domjur (11); Hugli: Goghat-I (27), Arambag (30), Chanditala-II (35), Serampur Uttarpara (36), Haripal (38); Nadia: Krishnagar-II (52), Haringhata (59), Tehatta-II (47), Tehatta-I (49), Chapra (51), Hanskhali (55); North 24 Parganas: Bagda (77), Gaighata (76), Habra-II (70), Bongaon (67), Swarupnagar (66) & South 24 Parganas: Magrahat-I (91), Sonarpur (84), Jaynagar-II (97), Diamond Harbour-II (79)	23
−41.9 to 0 (low)	Barddhaman: Kalna-II (10), Memari-II (1), Burdwan-II (8), Khandaghoṣh (3), Raina-II (4), Memari-I (9), Raina-I (6), Burdwan-I (5); Haora: Uluberia-II (20), Haroa (24), Uluberia-I (19), Udaynarayanpur (13), Panchla (21), Amta-I (15), Jagatballavpur (16), Shyampur-I (18), Amta-II (12), Sankrail (22); Hugli: Pursura (31), Goghat-II (26), Tarakeswar (33), Singur (37), Chinsurah-Magra (42), Chanditala-I (34), Jangipara (32), Hugli—Chinsurah (25), Balagarh (41), Khanakul-II (28), Dhaniakhali (39); Kolkata (43); Nadia: Chakdah (44), Krishnagar (53), Karimpur-II (46), Nakashipara (50); North 24 Parganas: Barasat (71), Barasat-II (72), Amdanga (73), Barrackpur-II (75), Habra-I (68), Minakhan (61), Barrackpur-I (74), Rajarhat (60), Hasnabad (62); South 24 Parganas: Budge Budge-I (82), Thakurpukur Mahestola (83), Bhangar-I (86), Bhangar-II (85), Bishnupur-II (89), Budge Budge-II (81), Falta (80), Baruiপুর (92) & Paschim Medinipur: Chandrakona-II (101), Garbeta-II (103), Garbeta-I (99)	54
0.1 to 15 (improvement)	Barddhaman: Jamalpur (7), Hugli: Pandua (40), Khanakul-I (29), Karimpur-I (45); South 24 Parganas: Jaynagar-I (78) & Paschim Medinipur: Ghatal (102), Chandrakona-I (98)	07
Total		93

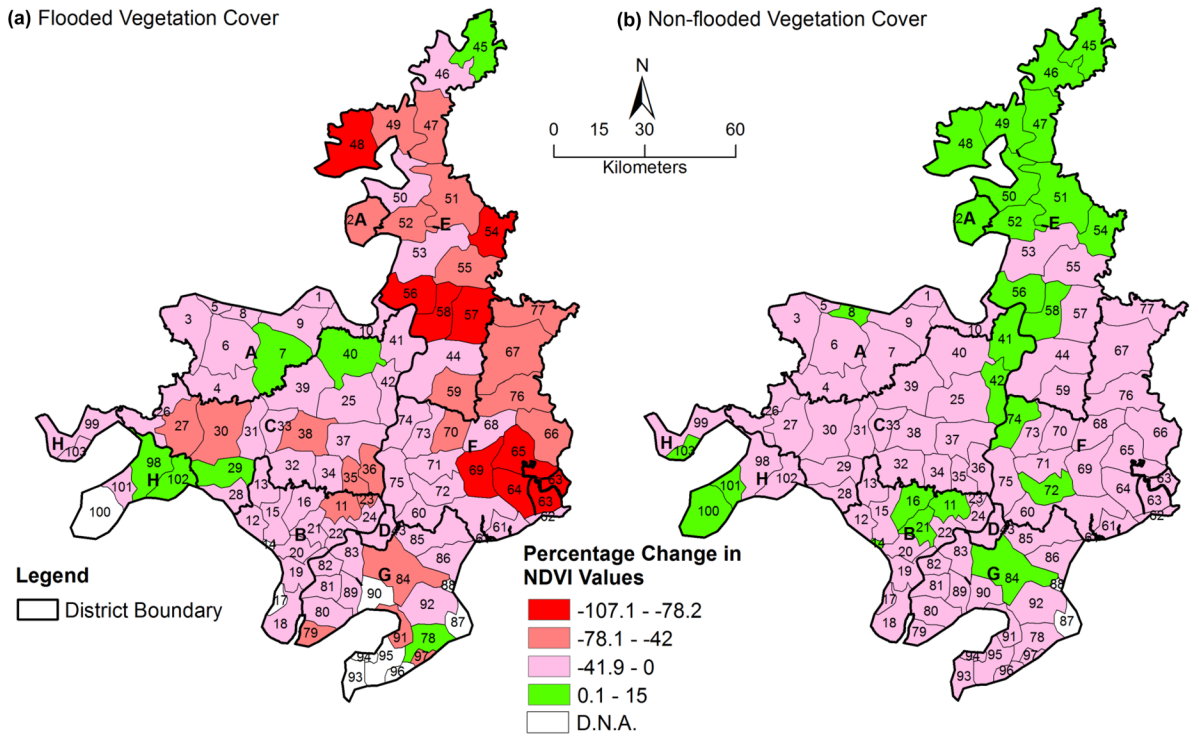


Fig. 10 Block-wise NDVI change in (a) flooded and (b) non-flooded vegetation cover. Label IDs A–H are denoting Bardhaman, Haora, Hugli, Kolkata, Nadia, North 24 Parganas, South 24 Parganas and Paschim Medinipur districts of W.B., respectively

Table 10 Percentage change in NDVI values of non-flooded vegetation cover of the cloud-free part of the study area

Percentage change in NDVI values	Non-flooded vegetation cover District: block name (Label ID)	No. of blocks
-107.1 to -78.2 (high)	N.A	N.A
-78.1 to -42 (moderate)	N.A	N.A
-41.9 to 0 (low)	Bardhaman: Khandaghosh (3), Raina-II (4), Raina-I (6), Burdwan-I (5), Memari-I (9), Jamalpur (7), Memari-II (1), Kalna-II (10); Haora: Shyampur-I (18), Bally Jagachha (23), Uluberia-I (19), Shyampur-II (17), Amta-II (12), Haroa (24), Uluberia-II (20), Udaynarayanpur (13), Amta-I (15), Sankrail (22); Hugli: Goghat-II (26), Chanditala-I (34), Haripal (38), Arambag (30), Serampur Uttarpara (36), Singur (37), Khanakul-II (28), Goghat-I (27), Jangipara (32), Chanditala-II (35), Dhaniakhali (39), Khanakul-I (29), Pandua (40), Tarakeswar (33), Pursura (31), Hugli- Chinsurah (25); Kolkata (43); Nadia: Haringhata (59), Ranaghat-II (57), Krishnagar (53), Chakdah (44), Hanskhali (55); North 24 Parganas: Basirhat-II (64), Baduria (65), Basirhat-I (63), Swarupnagar (66), Gaighata (76), De-ganga (69), Habra-I (68), Minakhan (61), Bongaon (67), Rajarhat (60), Bagda (77), Hasnabad (62), Habra-II (70), Amdanga (73), Barasat (71), Barrackpur-II (75); South 24 Parganas: Diamond Harbour-II (79), Budge Budge-I (82), Jaynagar-II (97), Kulpi (93), Mathurapur-I (96), Falta (80), Mandirbazar (95), Jaynagar-I (78), Magrahat-II (94), Bhangar-I (86), Bhangar-II (85), Budge Budge-II (81), Magrahat-I (91), Thakurpukur Mahestola (83), Bishnupur-II (89), Baruipur (92), Bishnupur-I (90) & Paschim Medinipur: Garbeta-I (99), Ghatal (102), Chandrakona-I (98)	76

Table 10 (Continued)

Percentage change in NDVI values	Non-flooded vegetation cover District: block name (Label ID)	No. of blocks
0.1 to 15 (improvement)	Bardhaman: Burdwan-II (8), Purbasthali-II (2); Haora: Domjur (11), Jagatballavpur (16), Panchla (21), Bagnan-I (14); Hugli: Chinsurah-Magra (42), Balagarh (41); Nadia: Santipur (56), Ranaghat-I (58), Karimpur-I (45), Krishnaganj (54), Kaliganj (48), Chapra (51), Krishnagar-II (52), Nakashipara (50), Tehatta-I (49), Karimpur-II (46), Tehatta-II (47); North 24 Parganas: Barrackpur-I (74), Barasat-II (72); South 24 Parganas: Sonarpur (84) & Paschim Medinipur: Keshpur (100), Garbeta-II (103), Chandrakona-II (101)	25
Total		101

Conclusions

The training site-based supervised threshold method is highly robust and operational for mapping the water pixels using Sentinel-1 SAR data. The present study demonstrated that Sentinel-1 SAR data have been efficiently captured the flooded areas near real-time while the Sentinel-2-based NDVI change is also showing promising results. Actual flooded and flood-affected cropland areas are highest in Purba Medinipur district. NDVI change analysis shows that the flooded cropland and vegetation cover is showing high reduction in NDVI values compared to non-flooded cropland and vegetation cover. The highest flood-affected built-up areas lie in North 24 Parganas. Since the built-up area in low-lying areas including Kolkata airport flooded due to Amphan-induced torrential rainfall, proper drainage plan and flood proofing measures should be implemented therein to avoid flooding in future. The geospatial approach discussed in this study to assess the impacts of Amphan cyclone can be further enhanced by using high-resolution satellite data and ground-based damage assessment of transport and communication infrastructure, built-up areas and cropland. This is one of the futuristic scopes of the present study. This study helps planners and policy makers to understand the district-wise flooding behavior, severity of damage to cropland and vegetation cover and to plan restriction on high-value land use (built-up) in flooded low lying areas.

Acknowledgements Authors are thankful to the European Space Agency (ESA) and United States Geological Survey (USGS) for providing satellite images at no cost. Authors acknowledge Ms. Ananya Pati, research scholar at Department of Oceanographic Studies, Jadavpur University, Kolkata (India) for providing field photographs. Authors also acknowledge

anonymous reviewers for their constructive comments that immensely improved the manuscript.

Data availability The datasets generated during and/or analysed during the current study are available from the corresponding author on reasonable request.

Declarations

Conflict of interest The authors declare no competing interests.

References

Agnihotri, A. K., Ohri, A., Gaur, S., Shivam, Das, N., & Mishra, S. (2019). Flood inundation mapping and monitoring using SAR data and its impact on Ramganga River in Ganga basin. *Environmental Monitoring and Assessment*, 191, 760. <https://doi.org/10.1007/s10661-019-7903-4>

Akram, S. K. W., Mondal, I., & Bandyopadhyay, J. (2019). Crop suitability analysis in water resource management of Paschim Medinipur District, India: a remote sensing approach. *Sustainable Water Resources Management*, 5, 797–815. <https://doi.org/10.1007/s40899-018-0262-4>

Alam, E., & Dominey-Howes, D. (2015). A new catalogue of tropical cyclones of the northern Bay of Bengal and the distribution and effects of selected landfalling events in Bangladesh. *International Journal of Climatology*, 35(6), 801–835. <https://doi.org/10.1002/joc.4035>

Ban, H. J., Kwon, Y. J., Shin, H., Ryu, H. S., & Hong S. (2017). Flood monitoring using satellite-based RGB composite imagery and refractive index retrieval in visible and near-infrared bands. *Remote Sensing*, 9(4), 313. <https://doi.org/10.3390/rs9040313>

Bhatt, C. M., Rao, G. S., & Jangam, S. (2020). Detection of urban flood inundation using RISAT-1 SAR images: A case study of Srinagar, Jammu and Kashmir (North India) floods of September 2014. *Modeling Earth Systems and Environment*, 6(1), 429–438. <https://doi.org/10.1007/s40808-019-00690-z>

Bhatt, C. M., Rao, G. S., Farooq, M., Manjusree, Shukla, A. P., Sharma, S. V. S. P., Kulkarni, S. S., Begum, A., Bhanumurthy V., Diwakar, P. G., & Dadhwal, V. K. (2016). Satellite-based

- assessment of the catastrophic Jhelum floods of September 2014, Jammu & Kashmir, India. *Geomatics, Natural Hazards and Risk*, 8(2), 309–327. <https://doi.org/10.1080/19475705.2016.1218943>
- Bhowmik, A. K., & Cabral, P. (2013). Cyclone Sidr impacts on the Sundarbans floristic diversity. *Earth Science Research*, 2(2), 62–79. <https://doi.org/10.5539/esr.v2n2p62>
- Clement, M. A., Kilsby, C. G., & Moore, P. (2018). Multi-temporal synthetic aperture radar flood mapping using change detection. *Journal of Flood Risk Management*, 11(2), 152–168. <https://doi.org/10.1111/jfr3.12303>
- Census of India. (2011a). Administrative atlas-West Bengal. Retrieved June 30, 2020, from <https://censusindia.gov.in/2011census/maps/atlas/West%20Bengal.html>
- Census of India. (2011b). District cesus handbook-West Bengal. Retrieved March 26, 2021, from <https://censusindia.gov.in/2011census/dchb/WB.html>
- Dodangeh, E., Choubin, B., Eigdir, A. N., Nabipour, N., Panahi, M., Shamshirband, S., & Mosavi, A. (2020). Integrated machine learning methods with resampling algorithms for flood susceptibility prediction. *Science of the Total Environment*, 705, 135983. <https://doi.org/10.1016/j.scitotenv.2019.135983>
- ESA. (2020a). Sentinel-2 mission details. Retrieved July 16, 2020, from <https://earth.esa.int/web/guest/missions/esa-operational-eo-missions/sentinel-2>
- ESA. (2020b). Multispectral instrument (MSI) overview. Retrieved July 16, 2020, from <https://earth.esa.int/web/sentinel/technical-guides/sentinel-2-msi/msi-instrument>
- ESA. (2020c). Sentinel-1 mission details. Retrieved July 16, 2020, from <https://earth.esa.int/web/guest/missions/esa-operational-eo-missions/sentinel-1>
- GKMS, & IMD. (2020). Special agro-met advispry service bulletin for the cyclone “Amphan”. Retrieved May 19, 2020, from <http://imd Kolkata.gov.in/acwc/fdpdata/view>
- Greenwood, F., Nelson, E. L., & Greenough, P. G. (2020). Flying into the hurricane: A case study of UAV use in damage assessment during the 2017 hurricanes in Texas and Florida. *PLoS ONE*, 15(2), e0227808. <https://doi.org/10.1371/journal.pone.0227808>
- GSI, & NRSC. (2012). Geomorphology and Lineament NGLM, Landform, 50K', West Bengal. Retrieved July 16, 2020, from <http://bhuvan.nrsc.gov.in/gis/thematic/index.php>
- Hoque, M. A. A., Phinn, S., Roelfsema, C., & Childs, I. (2016). Assessing tropical cyclone impacts using object-based moderate spatial resolution image analysis: A case study in Bangladesh. *International Journal of Remote Sensing*, 37(22), 5320–5343. <https://doi.org/10.1080/01431161.2016.1239286>
- Hu, T., & Smith, R. B. (2018). The impact of Hurricane Maria on the vegetation of Dominica and Puerto Rico using multispectral remote sensing. *Remote Sensing*, 10(6), 827. <https://doi.org/10.3390/rs10060827>
- IMD. (2020). All India weather summary. Retrieved May 21, 2020, from www.imdpune.gov.in
- Kumar, R. (2016). Flood hazard assessment of 2014 floods in Sonawari sub-district of Bandipore district (Jammu & Kashmir): An application of geoinformatics. *Remote Sensing Applications: Society and Environment*, 4, 188–203. <https://doi.org/10.1016/j.rsase.2016.10.002>
- Lin, T. C., Hogan, J. A., & Chang, C. T. (2020). Tropical cyclone ecology: A scale-link perspective. *Trends in Ecology and Evolution*. <https://doi.org/10.1016/j.tree.2020.02.012>
- Manavalan, R. (2017). SAR image analysis techniques for flood area mapping - literature survey. *Earth Science Informatics*, 10, 1–14. <https://doi.org/10.1007/s12145-016-0274-2>
- Mandal, M. S. H., & Hosaka, T. (2020). Assessing cyclone disturbances (1988–2016) in the Sundarbans mangrove forests using Landsat and Google Earth Engine. *Natural Hazards*, 102(1), 133–150. <https://doi.org/10.1007/s11069-020-03914-z>
- Manjusree, P., Bhatt, C. M., Begum, A., Rao, G. S., & Bhanumurthy, V. (2015). A decadal historical satellite data analysis for flood hazard evaluation: A case study of Bihar (North India). *Singapore Journal of Tropical Geography*, 36(3), 308–323. <https://doi.org/10.1111/sjtg.12126>
- Mason, D. C., Schumann, G. J. P., Neal, J. C., Garcia-Pintado, J., & Bates, P. D. (2012). Automatic near real-time selection of flood water levels from high resolution Synthetic Aperture Radar images for assimilation into hydraulic models: A case study. *Remote Sensing of Environment*, 124, 705–716. <https://doi.org/10.1016/j.rse.2012.06.017>
- Mishra, A. (2014). Temperature rise and trend of cyclones over the eastern coastal region of India. *Journal of Earth Science & Climatic Change*, 05(9), 227. <https://doi.org/10.4172/2157-7617.1000227>
- Mohapatra, M., Mandal, G. S., Bandyopadhyay, B. K., Tyagi, A., & Mohanty, U. C. (2012). Classification of cyclone hazard prone districts of India. *Natural Hazards*, 63, 1601–1620. <https://doi.org/10.1007/s11069-011-9891-8>
- NCRMP. (2020). Cyclones and their impact in India. Retrieved June 30, 2020, from <https://ncrmp.gov.in/cyclones-their-impact-in-india/>
- Negrón-Juárez, R., Baker, D. B., Chambers, J. Q., Hurtt, G. C., & Goosem, S. (2014). Multi-scale sensitivity of Landsat and MODIS to forest disturbance associated with tropical cyclones. *Remote Sensing of Environment*, 140, 679–689. <https://doi.org/10.1016/j.rse.2013.09.028>
- Neumann, C. J. (1993). Global overview. In *Global Guide to Tropical Cyclone Forecasting* (pp. 1.1–1.56). World Meteorological Organisation, Geneva.
- Pai, D. S., Sridhar, L., Rajeevan, M., Sreejith, O. P., Satbhai, N. S., & Mukhopadhyay, B. (2014). Development of a new high spatial resolution (0.25° × 0.25°) long period (1901–2010) daily gridded rainfall data set over India and its comparison with existing data sets over the region. *Mausam*, 65(1), 1–18.
- Pulvirenti, L., Chini, M., Pierdicca, N., & Boni, G. (2016). Use of SAR data for detecting floodwater in urban and agricultural areas: The role of the interferometric coherence. *IEEE Transactions on Geoscience and Remote Sensing*, 54(3), 1532–1544. <https://doi.org/10.1109/TGRS.2015.2482001>
- Ramsey, E. W., Hodgson, M. E., Sapkota, S. K., & Nelson, G. A. (2001). Forest impact estimated with NOAA AVHRR and landsat TM data related to an empirical hurricane wind-field distribution. *Remote Sensing of Environment*, 77(3), 279–292. [https://doi.org/10.1016/S0034-4257\(01\)00217-6](https://doi.org/10.1016/S0034-4257(01)00217-6)
- RSMC. (2020). Super cyclonic storm “APMPHAN” over the southeast Bay of Bengal (16th - 21st May 2020): summary. Retrieved July 10, 2020, from <http://www.rsmcnwdelhi>

- imd.gov.in/images/pdf/publications/preliminary-report/amphan.pdf
- Samanta, A. (1997). Cyclone hazards and community response in coastal West Bengal: An anthropo-historical perspective. *Economic and Political Weekly*, 32(38), 2424–2428.
- Schaefer, M., Teeuw, R., Day, S., Zekkos, D., Weber, P., Meredith, T., & Westen, C. J. V. (2020). Low-cost UAV surveys of hurricane damage in Dominica: automated processing with co-registration of pre-hurricane imagery for change analysis. *Natural Hazards*, 101, 755–784. <https://doi.org/10.1007/s11069-020-03893-1>
- Sebastian, M., & Behera, M. R. (2015). Impact of SST on tropical cyclones in North Indian Ocean. *Procedia Engineering*, 116, 1072–1077. <https://doi.org/10.1016/j.proeng.2015.08.346>
- Singh, L. P., Parkash, B., & Singhvi, A. K. (1998). Evolution of the lower gangetic plain landforms and soils in West Bengal India. *Catena*, 33(2), 75–104. [https://doi.org/10.1016/S0341-8162\(98\)00066-6](https://doi.org/10.1016/S0341-8162(98)00066-6)
- Singh, O. P., Ali Khan, T. M., & Rahman, M. S. (2000). Changes in the frequency of tropical cyclones over the North Indian Ocean. *Meteorology and Atmospheric Physics*, 75(1–2), 11–20. <https://doi.org/10.1007/s007030070011>
- Staben, G. W., & Evans, K. G. (2008). Estimates of tree canopy loss as a result of Cyclone Monica, in the Magela Creek catchment northern Australia. *Austral Ecology*, 33(4), 562–569. <https://doi.org/10.1111/j.1442-9993.2008.01911.x>
- State Inter Agency Group. (2020). Joint rapid need assessment report on cyclone Amphan. Retrieved March 25, 2021 from <https://nidm.gov.in/covid19/PDF/covid19/state/West%20Bengal/223.pdf>
- Tehrany, M. S., Pradhan, B., Mansor, S., & Ahmad, N. (2015). Flood susceptibility assessment using GIS based support vector machine model with different kernel types. *CATENA*, 125, 91–101. <https://doi.org/10.1016/j.catena.2014.10.017>
- Tiwari, V., Kumar, V., Matin, M. A., Thapa, A., Ellenburg, W. L., Gupta, N., & Thapa, S. (2020). Flood inundation mapping- Kerala 2018; Harnessing the power of SAR, automatic threshold detection method and Google Earth Engine. *PLoS One*, 15(8), e0237324. <https://doi.org/10.1371/journal.pone.0237324>
- Twele, A., Cao, W., Plank, S., & Martinis, S. (2016). Sentinel-1-based flood mapping: A fully automated processing chain. *International Journal of Remote Sensing*, 37(13), 2990–3004. <https://doi.org/10.1080/01431161.2016.1192304>
- UNICEF India. (2020). West Bengal Cyclone Amphan 2020, Situation Report 3. Retrieved June 30, 2020, from <https://reliefweb.int/sites/reliefweb.int/files/resources/UNICEF%20India%2C%20West%20Bengal%20Humanitarian%20Situation%20Report%20No.%203%2028Cyclone%20Amphan%29%20-%20for%2021%20May%202020.pdf>
- UN-SPIDER Knowledge Portal. (2021). Recommended Practice: Radar-based Flood Mapping. Retrieved March 25, 2021, from <https://www.un-spider.org/advisory-support/recommended-practices/recommended-practice-flood-mapping>
- Walcker, R., Laplanche, C., Herteman, M., Lambs, L., & Fromard, F. (2019). Damages caused by hurricane Irma in the human-degraded mangroves of Saint Martin (Caribbean). *Scientific Reports*, 9(1). <https://doi.org/10.1038/s41598-019-55393-3>
- WBDM-CDD. (2021). West Bengal Hazard Mapping : Cyclone. Retrieved March 26, 2021, from <http://wbmd.gov.in/Pages/cyclonemapping.aspx>
- WHO (World Health Organisation). (2020). Tropical cyclones. Retrieved May 06, 2020 from https://www.who.int/health-topics/tropical-cyclones#tab=tab_1
- WMO (World Meteorological Organisation). (2020). Tropical cyclones. Retrieved May 06, 2020 from <https://public.wmo.int/en/our-mandate/focus-areas/natural-hazards-and-disaster-risk-reduction/tropical-cyclones>
- World Bank. (2003). India financing rapid onset natural disaster losses in India: a risk management approach. Report no. 26844-IN. Retrieved May 06, 2020 from <http://documents.worldbank.org/curated/en/382141468759569928/pdf/268440IN.pdf>
- Zhang, X., Wang, Y., Jiang, H., & Wang, X. (2013). Remote-sensing assessment of forest damage by Typhoon Saomai and its related factors at landscape scale. *International Journal of Remote Sensing*, 34(21), 7874–7886. <https://doi.org/10.1080/01431161.2013.827344>

Publisher's Note Springer Nature remains neutral with regard to jurisdictional claims in published maps and institutional affiliations.